Research Square

Preprints are preliminary reports that have not undergone peer review.
They should not be considered conclusive, used to inform clinical practice,
or referenced by the media as validated information.

Beinaglutide modulates abdominal subcutaneous adipose tissue microenvironment and lipid metabolism in diet-induced obese mice: a multi-omics analysis

Lihua Zhou
Hebei North University
Weizheng Liang
Hebei North University
Yu Liu
Hebei North University
Zhuoran Wu
Hebei North University
Wenting Zhang
Hebei North University
Jinheng Li
Hebei North University
Junpu Feng
Hebei North University
Li Shi
only10556676260163.com

Aerospace Center Hospital
Mingxia Li
Hebei North University

Article

Keywords: Beinaglutide, GLP-1 receptor agonist, obesity, abdominal subcutaneous adipose tissue, multi-omics, lipid metabolism

Posted Date: October 19th, 2026

DOI: https://doi.org/10.21203/rs.3.rs-11093494/v1

License: This work is licensed under a Creative Commons Attribution 4.0 International License.
Read Full License

Additional Declarations: No competing interests reported.

Abstract

[Abstract]

Beinaglutide (BN), a recombinant human glucagon-like peptide-1 receptor agonist, exhibits beneficial effects on obesity and metabolic disorders; however, its effects on obesity-related adipose tissue alterations and molecular changes remain unclear. In this study, C57BL/6J mice were fed a high-fat diet (HFD) for 12 weeks to induce obesity, followed by 7 weeks of BN treatment. We evaluated metabolic phenotypes, serum biochemical parameters, adipose morphology, and abdominal subcutaneous adipose tissue using transcriptomic, proteomic, and untargeted metabolomic analyses. BN reduced body weight gain, improved glucose tolerance, partially ameliorated elevated liver enzyme levels, reduced selected adipose depot weights, and attenuated HFD-induced adipocyte hypertrophy. Transcriptomic analysis indicated that BN-associated genes were mainly related to inflammatory responses, extracellular matrix organization, cytoskeletal regulation, and immune processes. Proteomic and metabolomic analyses revealed changes in PPAR signaling, peroxisome function, fatty acid metabolism, membrane lipids, sphingolipids, unsaturated fatty acids, and acylcarnitine-related metabolites. Integrated multi-omics analysis identified Ppara, Fgf1, Serpine1, and Fn1 as candidate molecules linked to lipid metabolic alterations. These findings suggest that BN treatment is associated with partial improvement of HFD-induced metabolic dysfunction and adipose tissue abnormalities, accompanied by changes in inflammatory, extracellular matrix, and lipid metabolism-related processes.

1. Introduction

Obesity has emerged as a significant global public health challenge, with recent epidemiological data indicating that over one billion individuals worldwide were affected by obesity in 2022. Furthermore, the prevalence of obesity among adults has more than doubled since 1990[1, 2]. A core pathological mechanism underlying obesity is adipose tissue dysfunction, which functions not only as an energy storage organ but also as an endocrine regulator[3] and a critical mediator of immunometabolic regulation[4]. Prolonged nutrient excess leads to limited adaptive expansion capacity of adipose tissue, resulting in adipocyte hypertrophy and associated endoplasmic reticulum stress[5], chronic low-grade inflammation, and extracellular matrix (ECM) remodeling[6]. These pathological changes hinder the ability of adipose tissue to safely store excess lipids, prompting lipid redistribution to non-adipose tissues, such as the liver and skeletal muscle, and contributing to the development of insulin resistance, glucose and lipid metabolic disorders, and obesity-related metabolic complications[7, 8].

In recent years, glucagon-like peptide-1 receptor agonists (GLP-1RAs) have gained widespread use in the treatment of type 2 diabetes due to their glucose-dependent insulinotropic and glucose-lowering effects. As their additional actions, including inhibition of glucagon secretion, delayed gastric emptying, and regulation of central appetite networks, have been progressively elucidated, the clinical application of GLP-1RAs has expanded to include obesity and related metabolic diseases[9, 10]. Large-scale clinical studies have demonstrated that GLP-1RAs, such as semaglutide, can induce significant weight loss and

improve multiple cardiometabolic risk factors in individuals with overweight or obesity[11, 12]. Beyond the overall benefits in body weight and glycemic control, accumulating evidence suggests that GLP-1RAs may influence the functional state of adipose tissue, including fat distribution, adipocyte metabolism, lipid-handling capacity[13], and local inflammatory phenotypes[14]. These findings imply that metabolic benefits may not solely stem from reduced food intake and weight loss, but may also involve improvements in the adipose tissue microenvironment. Among existing GLP-1RAs, beinaglutide (BN), a recombinant human GLP-1 drug with high sequence homology to human GLP-1(7–36), exhibits pharmacokinetic characteristics that mimic the physiological secretion pattern of GLP-1[15]. Given its structural similarity and short-acting pharmacokinetic properties, BN presents a promising intervention model for observing adipose tissue responses that closely resemble endogenous GLP-1 signaling. While existing studies support the overall benefits of GLP-1RAs in obesity and metabolic abnormalities, systematic investigations into the effects of BN on pathological adipose tissue remodeling under obese conditions and its relationship with multi-omics changes in abdominal subcutaneous adipose tissue (SAT) remain limited.

Thus, this study established an HFD-induced obese mouse model and administered BN intervention to evaluate its effects on metabolic phenotypes and adipose tissue morphology. Additionally, transcriptomic, proteomic, and untargeted metabolomic changes in abdominal SAT were analyzed, with key genes validated through qPCR and Western blotting. This research aimed to characterize molecular changes in abdominal SAT following BN intervention and to provide multi-omics evidence for understanding its effects related to adipose tissue.

2. Research design and methods

2.1Animals, Diets and Beinaglutide Treatment

Four-week-old male specific pathogen-free C57BL/6J mice were obtained from Beijing SPF Biotechnology Co., Ltd. (Beijing, China; license No. SCXK [Jing] 2024-0001). Mice were housed in a temperature-controlled environment at 20 ± 5°C with 50–60% humidity, under a 12:12 h light/dark cycle, and had free access to food and water. They were randomly assigned to three groups: normal diet group (ND), high-fat diet group (HFD), and HFD plus BN treatment group (HFD + BN) (n = 10 per group). The HFD and low-fat control diet were procured from Beijing SPF Biotechnology Co., Ltd. Mice in the HFD and HFD + BN groups were fed an HFD (fat, Cat. No. D12492) for 12 weeks to induce obesity, while mice in the ND group received a low-fat control diet (Cat. No. D12450B).

Following obesity induction, mice in the HFD + BN group received the GLP-1 RA BN (Shanghai Benemae Pharmaceutical Corporation, Shanghai, China) at a dose of 150 μg/kg/day via subcutaneous injection in the back three times daily for 7 weeks. Mice in the ND and HFD groups received an equal volume of saline through subcutaneous injection at the same frequency. Body weight was monitored weekly. After 7 weeks of treatment, all mice were fasted for 12 hours with free access to water prior to sacrifice. Mice were euthanized by CO_2 inhalation in a closed chamber (purity ≥ 99%) was continuously introduced for 3

min, until respiratory arrest occurred. The procedure was conducted between 9:00 AM and 6:00 PM. Adipose tissues, including SAT, visceral adipose tissue (VAT), brown adipose tissue (BAT), and perirenal adipose tissue (PRAT), as well as livers, were rapidly collected, immediately frozen in liquid nitrogen, and stored at − 80°C for subsequent analysis.

All animal procedures adhered to guidelines for the care and use of laboratory animals and received approval from the Animal Ethics Committee of Hebei North University(HBNU20250422175)

2.2Metabolic phenotyping

Metabolic phenotypes were assessed via body weight measurement, glucose tolerance test (GTT), insulin tolerance test (ITT), and serum biochemical assays. Blood samples were allowed to stand at room temperature for 30 minutes and were then centrifuged at 3000 g for 10 minutes to obtain serum. Serum levels of glucose, triglycerides (TG), total cholesterol (CHOL), low-density lipoprotein cholesterol (LDL-C), high-density lipoprotein cholesterol (HDL-C), alanine aminotransferase (ALT), and aspartate aminotransferase (AST) were determined using an automated biochemical analyzer according to the manufacturer's instructions. To assess histopathological changes, liver and adipose tissue samples were fixed, embedded in paraffin, and sectioned to 7 μm and 6 μm thickness, respectively, followed by hematoxylin and eosin (H&E) staining. Representative images were captured under a light microscope, and adipocyte area was quantified using ImageJ software.

2.3Transcriptomic analysis

Total RNA was extracted from abdominal SAT using TRIzol reagent, following the manufacturer's protocol. RNA purity and concentration were assessed with a NanoDrop 2000 spectrophotometer, while RNA integrity was evaluated using an Agilent 2100 Bioanalyzer. mRNA was enriched from total RNA, and sequencing libraries were prepared using the VAHTS Universal V6 RNA-seq Library Prep Kit for Illumina according to the manufacturer's instructions. Qualified libraries were sequenced on an Illumina NovaSeq platform, generating 150-bp paired-end reads. Raw FASTQ reads were processed with Trimmomatic to eliminate low-quality reads, and gene counts were obtained using HTSeq-count. Differential expression analysis was performed with the DESeq package in R, considering genes with $P < 0.05$ and $|\log2(\text{fold change})| > 1$ as differentially expressed. Gene Ontology (GO) and Kyoto Encyclopedia of Genes and Genomes (KEGG) enrichment analyses were performed using the R/Bioconductor package clusterProfiler v2.4.2. Enrichment significance was evaluated using Fisher's exact test, and $P < 0.05$ was considered statistically significant.

2.4 Proteomic analysis

Abdominal subcutaneous adipose tissue was lysed in 8 M urea containing protease inhibitors, homogenized by sonication, and centrifuged at 15,000 × g for 10 min at 4°C. Protein concentrations were determined using a bicinchoninic acid assay. Proteins were reduced with dithiothreitol, alkylated with iodoacetamide, and digested with trypsin. The resulting peptides were acidified, desalted, and quantified.

Peptides were separated using a Vanquish Neo nanoLC system and analyzed on an Astral mass spectrometer in data-independent acquisition mode. Raw proteomic data were processed using DIA-NN.

Protein functional annotation was performed using Gene Ontology (GO), Kyoto Encyclopedia of Genes and Genomes (KEGG), and Pfam databases. GO annotation was performed using eggNOG-mapper v2.0. Protein domains were annotated using the Pfam database and PfamScan. For KEGG annotation, protein sequences were aligned against the KEGG database using BLASTp with an E-value threshold of ≤ 1 × 10 − 4, and the top-scoring match was selected for annotation.

KEGG pathway enrichment analysis of differentially expressed proteins was performed using Fisher's exact test, with all identified proteins used as the background set. A P value < 0.05 was considered statistically significant.

2.5 Metabolomic analysis

Metabolites were extracted from approximately 5 mg of frozen abdominal SAT using 80% methanol containing internal standards. Pooled quality control samples were prepared by mixing equal aliquots from all extracts. After centrifugation, the supernatants were lyophilized, reconstituted in 10% methanol, and analyzed using a Q Exactive HF-X mass spectrometer coupled with a Vanquish Flex UPLC system. Raw data were processed with XCMS and Spectra, and metabolites were annotated using public databases. Differential metabolites were identified by t-test and OPLS-DA (VIP > 1, P < 0.05). KEGG enrichment analysis was performed using Fisher's exact test.

2.6 Quantitative real-time PCR (qPCR) validation

Total RNA was extracted from abdominal SAT, and according to the manufacturer's instructions, the extracted RNA was reverse-transcribed into complementary DNA (cDNA) using a reverse transcription kit. Quantitative real-time PCR was conducted with gene-specific primers and SuperReal PreMix Plus (SYBR Green) (FP205-02), using cDNA as the template. The expression levels of all target genes were normalized to the endogenous control β-actin. The primer sequences utilized in this study are listed in Table S1.

2.7 Western blot validation

Abdominal SAT samples were lysed in RIPA buffer supplemented with PMSF for protein extraction. Following complete lysis, the samples were centrifuged at 12,000 g for 30 minutes at 4°C, and the supernatants were collected. Protein concentrations were determined using the Bradford assay. Equal amounts of protein were mixed with SDS loading buffer and boiled for 5 minutes. Proteins were then separated by SDS-PAGE and transferred onto PVDF membranes. Post-transfer, the membranes were blocked with 5% non-fat milk at room temperature for 1 hour and incubated with primary antibodies overnight at 4°C. After washing, the membranes were incubated with secondary antibodies at room temperature for 1 hour. Protein bands were visualized using enhanced chemiluminescence reagents and captured with a chemiluminescence imaging system. Band intensities were quantified using image analysis software and normalized to β-actin.

2.8 Multi-omics integration

KEGG enrichment results from the transcriptomic, proteomic, and metabolomic analyses were intersected to identify pathways shared across the three omics layers. Shared pathways were visualized using a Venn diagram and a grouped bubble plot based on enrichment statistics from the HFD + BN vs HFD comparison. Candidate genes were selected based on shared pathway annotations, transcriptomic expression trends, and biological relevance to lipid metabolism, inflammation, and ECM remodeling. Pearson correlation analysis was conducted between normalized DEGs levels and differential metabolite abundances. Correlations with $|r| \geq 0.8$ and $P < 0.05$ were used to construct the gene-metabolite network.

2.9 Statistical analysis

Statistical analyses were performed using GraphPad Prism 8.0 (GraphPad Software, Boston, MA, USA). Data are presented as mean ± standard error of the mean (mean ± SEM). Comparisons among multiple groups were analyzed via one-way ANOVA or two-way repeated-measures ANOVA as appropriate. When ANOVA revealed significant differences, Tukey's honestly significant difference (HSD) post hoc test was applied for pairwise comparisons

3. Results

3.1 Beinaglutide improves obesity-associated metabolic phenotypes in HFD-fed mice

To evaluate the effect of BN on diet-induced obesity, an HFD-induced obesity model was established in C57BL/6J mice. Following 12 weeks of HFD feeding, mice received BN at a dose of 150 μg/kg/day for 7 weeks (Fig. 1A). HFD-fed mice exhibited an enlarged body size compared to ND-fed mice, while BN-treated mice had a body size comparable to that of ND mice (Fig. 1B). During the modeling period, body weight progressively increased in the HFD group, surpassing that of the ND group from week 3 onward (Fig. 1C). Throughout the intervention period, body weight gain was suppressed in the HFD + BN group compared to the HFD group, indicating that BN mitigated further HFD-associated weight gain (Fig. 1D). Further assessment of glucose metabolism revealed that the GTT indicated improved glucose tolerance in BN-treated obese mice compared to HFD mice (Fig. 1E). In contrast, the ITT showed that BN treatment did not significantly alter the ITT-AUC in HFD mice, suggesting that the improvement in systemic insulin sensitivity by BN was limited and did not reach a significant level (Fig. 1F).

Serum levels of ALT, AST, total CHOL, TG, HDL-C, and LDL-C were measured. Compared to the ND group, HFD-fed mice displayed elevated ALT levels alongside a modest increase in AST. BN treatment resulted in reduced ALT levels relative to the HFD group, while AST levels showed a non-significant decrease (Fig. 1G). Regarding the lipid profile, HFD feeding increased CHOL levels without significantly affecting TG, HDL, or LDL levels. BN administration did not significantly influence any of the measured lipid parameters (CHOL, TG, HDL, or LDL) compared to the HFD group (Fig. 1H).

3.2Beinaglutide Improves HFD-Induced Morphological Abnormalities in Adipose Tissue

To further evaluate the effects of BN on HFD-induced adipose tissue remodeling, adipose tissue weights and HE-stained morphology were analyzed. Representative gross images of SAT, VAT, BAT, and PRAT from the three groups are shown in (Fig. 2A). Tissue weight analysis indicated that HFD significantly increased the weights of SAT, VAT, and PRAT; however, BN intervention led to a significant reduction in the weights of VAT, BAT, and PRAT, While SAT weight showed a decreasing trend post-BN intervention, this difference was not statistically significant compared to the HFD group (Fig. 2B).

HE staining demonstrated that HFD induced morphological alterations in multiple adipose tissues, including enlarged adipocytes in SAT, VAT, and PRAT, as well as enlarged lipid vacuoles within brown adipocytes; these changes were alleviated following BN intervention (Fig. 2C). Quantitative analysis revealed that the mean adipocyte area in SAT significantly increased in the HFD group relative to the ND group, whereas BN intervention significantly reduced the mean adipocyte area in SAT (Fig. 2D). In VAT and PRAT, adipocyte area also significantly increased in the HFD group compared to the ND group, and after BN intervention, adipocyte area in VAT and PRAT did not change significantly(Fig. 2E, F). In BAT, adipocyte area was enlarged, and intracellular lipid vacuoles were larger in the HFD group compared to the ND group; BN intervention significantly reduced BAT adipocyte area relative to the HFD group (Fig. 2G). Overall, BN intervention improved HFD-induced adipose tissue abnormalities by reducing the weights of certain adipose depots and attenuating adipocyte hypertrophy.

3.3 Beinaglutide treatment ameliorates inflammation and extracellular matrix remodeling in abdominal subcutaneous adipose tissue.

To investigate whether the amelioration of HFD-induced metabolic abnormalities by BN was accompanied by changes in the transcriptional state of abdominal SAT, transcriptomic analysis was performed, focusing on DEGs and their functional enrichment characteristics. Differential expression analysis revealed that, compared to the ND group, 912 genes were differentially expressed in the HFD group, including 503 upregulated and 409 downregulated genes. In the HFD + BN group, 1118 genes were differentially expressed compared to the HFD group, comprising 511 upregulated and 607 downregulated genes (Fig. 3A, B). A total of 250 DEGs overlapped between the two comparisons (Fig. 3C).

To determine whether these transcriptional changes were associated with the pathological state of obese adipose tissue, visualization of representative genes altered by HFD and showing a trend toward reversal after BN intervention was performed. The heatmap indicated that a set of genes related to the ECM, inflammatory response, cell adhesion, and tissue remodeling were generally upregulated in the HFD group, while their expression decreased to varying degrees after BN treatment, including *Serpine1*, *Fn1*, *Fgf1*, *Hspg2*, *Col12a1*, and *Col16a1* (Fig. 3D).

Functional enrichment analysis revealed distinct transcriptional features associated with HFD and BN intervention. The DEGs from the HFD vs ND comparison were primarily enriched in KEGG pathways such as fatty acid metabolism, carbon metabolism, pyruvate metabolism, tricarboxylic acid (TCA) cycle, and fatty acid elongation. GO analysis indicated that these genes were associated with processes related to fatty acid metabolism, acyl-CoA metabolism, acetyl-CoA metabolism, the generation of precursor metabolites and energy, and the mitochondrial matrix (Fig. 3E). In contrast, DEGs in the HFD + BN vs HFD comparison were prominently enriched in pathways related to inflammation and the tissue microenvironment, including the AGE-RAGE signaling pathway, NF-kappa B signaling pathway, ECM-receptor interaction, chemokine signaling pathway, and regulation of the actin cytoskeleton. GO analysis further revealed that BN-associated DEGs were involved in processes such as regulation of inflammatory response, production of inflammation-related cytokines, NLRP3 inflammasome complex assembly, ECM organization, actin filament organization, collagen-containing ECM, focal adhesion, integrin binding, and immune receptor activity (Fig. 3F). These results indicate that the DEGs following BN intervention were primarily associated with changes in inflammatory responses and ECM remodeling.

3.4 Proteomics reveals that BN treatment alters the PPAR/oxidative enzyme bodies and fatty acid oxidation-related pathways in subcutaneous fat

To further characterize the functional state of adipose tissue post-BN intervention at the protein level, proteomic analysis of abdominal SAT was performed. Differential protein expression analysis revealed that, compared to the ND group, 285 proteins were differentially expressed in the HFD group, with 111 upregulated and 174 downregulated proteins. In the HFD + BN group, 1044 proteins were differentially expressed compared to the HFD group, including 592 upregulated and 452 downregulated proteins (Fig. 4A, B). A total of 60 differentially expressed proteins overlapped between the two comparisons (Fig. 4C).

Heatmap analysis of representative proteins indicated that a group of proteins related to immune response, cell adhesion, and matrix remodeling tended to be increased in the HFD group, including Serpine1, Fn1, Fbln2, Thbs1, Itgb1, Cd44, and Fgf1. Following BN intervention, these proteins generally decreased to varying degrees. Conversely, several proteins associated with fatty acid oxidation, mitochondrial function, and peroxisomes tended to increase after BN intervention, including Acox1, Acsl1, Ehhadh, Hsd17b4, Cpt2, Acadm, Acadl, Pex3, and Pex16 (Fig. 4D).

KEGG enrichment analysis demonstrated that differentially expressed proteins in the HFD vs ND comparison were enriched in pathways such as ECM-receptor interaction, neutrophil extracellular trap formation, leukocyte transendothelial migration, complement and coagulation cascades, cell adhesion molecules, focal adhesion, and regulation of the actin cytoskeleton (Fig. 4E). In contrast, differentially expressed proteins in the HFD + BN vs HFD comparison were enriched in pathways related to the PPAR signaling pathway, peroxisome, fatty acid degradation, TCA cycle, pyruvate metabolism, oxidative phosphorylation, thermogenesis, and glycerophospholipid/ether lipid metabolism (Fig. 4F). These

findings suggest that BN intervention promotes lipid oxidation, energy metabolism, and membrane lipid metabolism.

3.5Metabolomics reveals BN-associated changes in lipid metabolism in abdominal subcutaneous adipose tissue

To further evaluate whether BN intervention was associated with changes in the metabolic state of abdominal SAT, untargeted metabolomic analysis was conducted on samples from each group. OPLS-DA analysis demonstrated distinguishable metabolic profile distributions between the HFD and ND groups, as well as the HFD + BN and HFD groups (Fig. 5A, B). Differential metabolite analysis revealed that, compared to the ND group, 448 metabolites were altered in the HFD group, with 219 upregulated and 229 downregulated metabolites. In the HFD + BN group, 381 metabolites were altered compared to the HFD group, including 229 upregulated and 152 downregulated metabolites (Fig. 5C, D). Venn analysis identified 144 differential metabolites that overlapped between the two comparisons (Fig. 5E).

The metabolite heatmap indicated that HFD-induced metabolic alterations involved various classes of lipids and small-molecule metabolites, such as phosphatidylcholines (PC), phosphatidylethanolamines (PE), sphingolipids, lysophospholipids, unsaturated fatty acids, and acylcarnitine-related metabolites. Following BN intervention, these metabolites were re-regulated to varying degrees, particularly PC, PE, sphingomyelin (SM), lysophosphatidylinositol (LPI), lysophosphatidylglycerol (LPG), docosahexaenoic acid, dicarboxylic acids, and acylcarnitine-related molecules (Fig. 5F).

KEGG pathway analysis indicated that HFD-induced differential metabolites were primarily involved in sphingolipid metabolism, glycerophospholipid metabolism, biosynthesis of unsaturated fatty acids, fatty acid degradation, and carbon metabolism (Fig. 5G). In contrast, differential metabolites after BN intervention were mainly associated with pathways such as the sphingolipid signaling pathway, sphingolipid metabolism, glycerophospholipid metabolism, biosynthesis of unsaturated fatty acids, regulation of lipolysis in adipocytes, and arachidonic acid metabolism (Fig. 5H). These findings suggest that BN intervention was associated with significant changes in membrane lipid composition, sphingolipid signaling, and unsaturated fatty acid metabolism in abdominal SAT

3.6 Multi-omics integrated analysis suggests that adipose tissue remodeling after BN intervention is associated with lipid metabolism

To determine whether BN-associated changes revealed by transcriptomic, proteomic, and metabolomic analyses indicated common biological processes, an integrative intersection analysis of KEGG enrichment results from the three omics datasets was performed. Venn analysis identified 17 KEGG pathways overlapping among the transcriptome, proteome, and metabolome datasets (Fig. 6A). Further grouped visualization of these shared pathways based on enrichment statistics from the BN intervention-related comparison (HFD + BN vs HFD) showed their involvement in membrane lipid and inflammatory lipid metabolism, metabolic stress/cellular injury responses, as well as amino acid and small-molecule metabolic processes. These pathways included glycerophospholipid metabolism, ether

lipid metabolism, arachidonic acid metabolism, AGE-RAGE signaling pathway in diabetic complications, necroptosis, chemical carcinogenesis-reactive oxygen species, glycine, serine and threonine metabolism, and tryptophan metabolism (Fig. 6B).

Focusing on biological processes related to lipid metabolic remodeling, metabolic stress, and the inflammatory-ECM microenvironment among the shared pathways across the three omics datasets—along with genes induced by HFD and reversed after BN intervention from the transcriptomic analysis—*Ppara*, *Fgf1*, *Serpine1*, and *Fn1* were identified as candidate nodes. These genes correspond to the fatty acid oxidation/PPAR axis, adipose tissue remodeling, and ECM/inflammatory microenvironment-related processes.

Correlations between key genes and differential metabolites were subsequently analyzed. The correlation heatmap displayed modular correlation patterns between candidate genes and adipose tissue microenvironment-related genes with various classes of lipid metabolites, particularly those related to acylcarnitines, sphingolipids, ether lipids, and membrane phospholipids (Fig. 6C). The gene-metabolite correlation network revealed that *Fgf1* and *Serpine1* formed concentrated association modules with multiple lipid metabolites, including Icosa-8,11,14-trienoylcarnitine, phytosphingosine, SM 8:0;2O/34:4, and several PE-related metabolites (Fig. 6D). Overall, changes in abdominal SAT after BN intervention primarily focused on lipid metabolism, the inflammatory-ECM microenvironment, and metabolic stress-related processes. *Ppara*, *Fgf1*, *Serpine1*, and *Fn1* may link these transcriptional changes with metabolic alterations.

3.7 Fgf1- and Serpine1-Associated Metabolic Correlations and Validation of Candidate Molecules

Based on the preceding multi-omics integrative analysis and the gene-metabolite correlation network, representative Fgf1- and Serpine1-associated gene-metabolite pairs were selected for scatter plot analysis. Seven representative correlations involving long-chain acylcarnitines, sphingolipids, sphingomyelins, and ether phospholipid-related metabolites were identified. Among these, Fgf1 exhibited a negative correlation with Icosa-8,11,14-trienoylcarnitine and a positive correlation with phytosphingosine, while Serpine1 also showed a negative correlation with Icosa-8,11,14-trienoylcarnitine (Fig. 7A, B). Furthermore, Fgf1 and Serpine1 correlated with membrane lipid-related molecules such as SM 8:0;2O/34:4 and PE O-16:1/20:4.

The expression of candidate genes was validated using RT-qPCR. Results indicated a decrease in Ppara expression in the HFD group compared to the ND group, whereas Serpine1, Fn1, and Fgf1 expressions increased. Following BN intervention, Ppara expression was upregulated, while Serpine1, Fn1, and Fgf1 expressions decreased (Fig. 7C-F). These changes were consistent with the transcriptomic analysis outcomes.

Western blot analysis revealed decreased PPARα protein expression in the HFD group, while FN1, SERPINE1, and FGF1 protein expressions were increased. After BN intervention, these protein expression

changes exhibited the opposite trend (Fig. 7G-K). These results indicate that candidate molecules related to PPARα-associated lipid metabolism, ECM remodeling, and the inflammatory microenvironment in abdominal SAT were re-regulated after BN intervention, supporting findings

from the multi-omics analyses.

4. Discussion

As a recombinant human GLP-1, BN has demonstrated the ability to reduce body weight, fat mass, and lipid levels in HFD-induced obese mice, while also regulating the lipid composition of adipose tissue and the expression of lipid metabolism-related genes[13]. Building on this, the current study found that BN intervention alleviated metabolic abnormalities and pathological changes in adipose tissue induced by HFD, as well as remodeled the multi-level molecular state of abdominal SAT. Overall, the response of subcutaneous fat to BN intervention extended beyond a single metabolic pathway, indicating a coordinated regulation of lipid metabolism, inflammation, and the ECM microenvironment.

At the phenotypic level, this study demonstrated that BN treatment attenuated body weight gain in HFD-fed mice and partially improved glucose intolerance and selected liver function-related parameters, suggesting that BN mitigates HFD-induced obesity-associated metabolic disturbances. These findings align with previous research on other GLP-1 RAs[16]. Histological analysis of adipose tissue using H&E staining indicated that HFD feeding induced marked adipocyte hypertrophy, while adipocyte size exhibited a decreasing trend following BN treatment. Given that adipocyte hypertrophy is closely linked to lipid storage stress, dysregulated lipolysis, and metabolic dysfunction[17, 18], these findings suggest that BN may aid in improving structural abnormalities in adipose tissue under obese conditions. Notably, although BN improved glucose tolerance and reduced subcutaneous adipocyte hypertrophy, it did not significantly enhance systemic insulin sensitivity (as assessed by ITT-AUC), circulating lipid profiles (TG and LDL-C), or morphological alterations in VAT and PRAT within the current 7-week intervention period. These results imply that different tissues and adipose depots may exhibit varying responsiveness to BN treatment, with abdominal SAT likely demonstrating greater adaptive changes in response to GLP-1 receptor activation compared to visceral fat depots. Alternatively, prolonged treatment durations may be necessary to achieve broader systemic metabolic benefits.

In obesity, adipose tissue is frequently associated with immune cell infiltration, chronic low-grade inflammation, ECM deposition, and fibrosis-like remodeling. These changes impair the healthy lipid storage capacity of adipose tissue and contribute to metabolic dysfunction[7, 19, 20].Consistent with this pathological context, the transcriptomic analysis in this study revealed that, under HFD conditions, genes related to inflammatory responses, ECM organization, cell adhesion, and tissue structural regulation were altered in abdominal SAT. Following BN intervention, the expression patterns of these genes changed correspondingly. Previous studies have indicated that macrophage remodeling and inflammatory activation within adipose tissue during obesity are closely associated with insulin resistance and metabolic dysfunction[21–23].Additionally, excessive ECM deposition and fibrosis-like

changes can restrict the adaptive expansion of adipose tissue, exacerbating metabolic issues[21, 24].Thus, the transcriptional changes observed after BN intervention may reflect multiple molecular processes associated with inflammation and ECM-related pathways, rather than changes in a single gene alone.

Dysfunction of obese adipose tissue entails not only inflammation and ECM alterations but is also closely tied to its capacity for lipid storage and release, insulin sensitivity, and related metabolic functions[25, 26]. Based on this rationale, the present study integrated proteomic and metabolomic results to assess whether BN intervention was associated with coordinated changes at the metabolic level. Proteomic analysis indicated that differentially expressed proteins after BN intervention mainly converged on processes such as fatty acid oxidation, peroxisomal function, PPAR-related lipid metabolism, and oxidative phosphorylation, suggesting that BN-associated responses may involve the re-regulation of energy metabolism and lipid-handling networks in adipose tissue. Supporting this interpretation, recent studies have demonstrated that peroxisomal lipid synthesis in adipose tissue can influence obesity and insulin resistance through LXR-dependent lipogenesis[27]. Additionally, metabolic pathways such as fatty acid oxidation are altered in adipose tissue under obese conditions, with activation of the adipose tissue ATGL-PPARα pathway linked to improvements in HFD-induced obesity, energy expenditure, and insulin sensitivity[28].

Consistently, metabolomic analysis revealed that several classes of lipid-related metabolites in abdominal SAT were altered after BN intervention, primarily involving membrane lipid metabolism, sphingolipid signaling, unsaturated fatty acid metabolism, and processes related to fatty acid oxidation. Integrative analysis of proteomic and metabolomic data suggested that BN intervention was associated with modifications in molecular features related to lipid metabolism and energy metabolism in abdominal SAT, indicating that BN may influence adipose tissue-related metabolic processes. These findings align with previous observations that BN can affect lipid composition and the expression of lipid metabolism-related genes in adipose tissue[13].

Based on the transcriptomic, proteomic, and metabolomic results, multi-omics integration and gene-metabolite correlation analysis were conducted to identify candidate molecules involved in inflammatory-related, ECM-related, and lipid metabolism-related processes. Shared pathway analysis revealed that the molecular changes in abdominal SAT after BN intervention were primarily linked to lipid metabolism, energy metabolism, inflammatory responses, and ECM-related processes. Examining the expression of DEGs in the transcriptome, the common pathway results from the three omics analyses, and validation of select differentially expressed molecules by qPCR and Western blotting, Ppara, Fgf1, Serpine1, and Fn1 were identified as candidate genes warranting further investigation. This selection is supported by previous literature, which indicates that semaglutide upregulates *Ppar*α and genes related to browning/mitochondrial biogenesis in subcutaneous WAT of HFD-induced obese mice while alleviating adipose tissue hypertrophy and inflammatory responses[29]. FGF1 serves as a downstream regulator of PPARγ, participating in the adaptive remodeling of WAT under energy excess conditions and helping maintain glucose and lipid metabolic homeostasis[30, 31]. *SERPINE1* encodes PAI-1, an inhibitor

of the fibrinolytic system, and is associated with fibrosis and ECM remodeling in obese adipose tissue[32]. *FN1* encodes fibronectin, an important component of ECM deposition and cell-matrix adhesion; ECM components like fibronectin are upregulated in WAT from obese mice and humans, and ECM genes are linked to metabolic indicators such as blood lipids and glucose levels[33]. The findings from previous studies are consistent with the biological functions associated with these candidate molecules. Nonetheless, whether these molecules directly mediate BN-induced changes in adipose tissue remains to be validated through functional experiments.

Further gene-metabolite correlation analysis revealed significant associations between Fgf1 and Serpine1 expression and metabolites related to acylcarnitines, sphingolipids, and membrane phospholipids. Previous studies indicated that acylcarnitines reflect fatty acid transport, mitochondrial β-oxidation activity, and metabolic stress[34]. In the context of obesity and insulin resistance, circulating acylcarnitine profiles may indicate obesity-related mitochondrial metabolic burden, with liraglutide treatment associated with improvements in these profiles[35]. Additionally, abnormalities in sphingolipid and ceramide metabolism are linked to inflammation- and lipid overload-related insulin resistance[36, 37], while changes in membrane phospholipid composition relate to cell membrane structure, lipid droplet storage, and regulation of lipid signaling[38, 39]. Taken together, alterations in Fgf1 and Serpine1 may be implicated in inflammation-related and lipid metabolism-related molecular changes in adipose tissue following BN intervention.

The choice of experimental model is also crucial when interpreting these findings. This study utilized male C57BL/6J mice to establish an obesity model induced by an HFD. C57BL/6J mice are commonly used experimental animals in obesity and metabolic disease research, demonstrating stable weight gain, fat accumulation, and associated metabolic abnormalities under HFD stimulation[40]. Moreover, the use of male mice can reduce the potential influence of sex hormone cycle variations on metabolic phenotype evaluations.

This study has several limitations. First, as a discovery-based multi-omics study, the findings are primarily correlative; gain- or loss-of-function experiments were not conducted to validate the causal roles of Ppara, Fgf1, or Serpine1 in mediating BN's effects. Second, the cellular heterogeneity of adipose tissue was not deconvoluted, leaving the specific cell types responsible for the observed transcriptional and proteomic shifts unidentified. Third, the molecular mechanisms underlying the differential responses between subcutaneous and visceral adipose tissues require further investigation using complementary approaches.

5. Conclusions

The present study demonstrates that BN alleviated HFD-induced obesity-related metabolic abnormalities and improved morphological alterations in adipose tissue. Multi-omics analyses of abdominal SAT revealed that transcriptional changes following BN intervention were primarily linked to inflammation-related and ECM-related processes. Concurrently, proteomic and metabolomic analyses suggested

alterations in lipid metabolism, energy metabolism, and membrane lipid-related metabolic processes. Integrated multi-omics analysis identified Ppara, Fgf1, Serpine1, and Fn1 as candidate hub molecules exhibiting significant correlations with specific lipid metabolites. While these genes are recognized regulators of adipose tissue fibrosis and metabolism, the current observational study cannot establish causality regarding their role in mediating BN's effects. Future studies involving adipose-specific genetic manipulation are necessary to determine whether these molecules act as upstream targets or downstream effectors of BN-induced metabolic remodeling.

Abbreviation

BN Beinaglutide

GLP-1 Glucagon-like peptide-1

GLP-1RA Glucagon-like peptide-1 receptor agonist

HFD High-fat diet

ND Normal diet

SAT Subcutaneous white adipose tissue

VAT Visceral adipose tissue

BAT Brown adipose tissue

PRAT Perirenal adipose tissue

GTT Glucose tolerance test

ITT Insulin tolerance test

HDL-C High-density lipoprotein cholesterol

LDL-C Low-density lipoprotein cholesterol

DEGs Differentially expressed genes

DEPs Differentially expressed proteins

ECM Extracellular matrix

KEGG Kyoto Encyclopedia of Genes and Genomes

OPLS-DA Orthogonal partial least-squares discriminant analysis

Declarations

Ethics approval and consent to participate

All animal procedures adhered to guidelines for the care and use of laboratory animals and received approval from the Animal Ethics Committee of Hebei North University(HBNU20250422175)

Consent for publication

Not applicable.

Conflict of interest statement

The authors have no conflicts of interest to declare.

Funding Sources

This research was supported by the Capacity Building and Continuing Education Center of the National Health Commission (2025 Special Research Project in Pediatrics and Pharmacy, GWJJZX20251001047) and the Hebei Provincial Natural Science Foundation (Precision Medicine Innovation Development Joint Fund Cultivation Project, H2025405024).

Author Contribution

L.S. and Y.L. conceptualized the study. L.Z., W.L., and Y.L. designed the methodology. L.Z. and Z.W. developed the software and performed visualization. Validation was carried out by L.Z., W.Z., and J.L., while formal analysis was conducted by L.Z., W.L., and Z.W. The investigation was performed by L.Z., Y.L., W.Z., J.L., and J.F. Resources and funding were provided by L.S. and M.L. Data curation was handled by L.Z. and Y.L. The original draft was prepared by L.Z., and the manuscript was reviewed and edited by L.S. and Y.L. Supervision, project administration, and funding acquisition were overseen by L.S. and M.L. All authors have read and agreed to the published version of the manuscript.

Acknowledgement

We thank Bullet Edits Limited for the linguistic editing and proofreading of the manuscript.

Data Availability

The transcriptomic data generated in this study have been deposited in the NCBI Gene Expression Omnibus (GEO) under accession number GSE347087 and are publicly available

at:https://www.ncbi.nlm.nih.gov/geo/query/acc.cgi?acc=GSE347087The mass spectrometry proteomics data have been deposited to the ProteomeXchange Consortium via the iProX partner repository under dataset identifier PXD084126. The dataset is publicly available at:https://proteomecentral.proteomexchange.org/cgi/GetDataset?ID=PXD084126The corresponding iProX project is available at:https://www.iprox.cn/page/project.html?id=IPX0019599000The metabolomics data have been deposited in the MetaboLights repository under study identifier MTBLS15659 and are publicly available at:https://www.ebi.ac.uk/metabolights/MTBLS15659

References

1. Organization, W. H. *Obesity and overweight*, (2025). https://www.who.i-nt/news-room/fact-sheets/detail/obesity-and-overweight
2. Phelps, N. H. et al. Worldwide trends in underweight and obesity from 1990 to 2022: a pooled analysis of 3663 population-representative studies with 222 million children, adolescents, and adults. *Lancet* **403**, 1027–1050. 10.1016/S0140-6736(23)02750-2 (2024).
3. Reyes-Farias, M., Fos-Domenech, J., Serra, D., Herrero, L. & Sanchez-Infantes, D. White adipose tissue dysfunction in obesity and aging. *Biochem. Pharmacol.* **192**, 114723. 10.1016/j.bcp.2021.114723 (2021).
4. Nance, S. A., Muir, L. & Lumeng, C. Adipose tissue macrophages: Regulators of adipose tissue immunometabolism during obesity. *Mol. Metab.* **66**, 101642. 10.1016/j.molmet.2022.101642 (2022).
5. Ma, K., Zhang, Y., Zhao, J., Zhou, L. & Li, M. Endoplasmic reticulum stress: bridging inflammation and obesity-associated adipose tissue. *Front. Immunol.* **15**, 1381227. 10.3389/fimmu.2024.1381227 (2024).
6. Dahdah, N., Tercero-Alcazar, C., Malagon, M. M., Garcia-Roves, P. M. & Guzman-Ruiz, R. Interrelation of adipose tissue macrophages and fibrosis in obesity. *Biochem. Pharmacol.* **225**, 116324. 10.1016/j.bcp.2024.116324 (2024).
7. Marcelin, G., Gautier, E. L. & Clement, K. Adipose Tissue Fibrosis in Obesity: Etiology and Challenges. *Annu. Rev. Physiol.* **84**, 135–155. 10.1146/annurev-physiol-060721-092930 (2022).
8. Bluher, M. An overview of obesity-related complications: The epidemiological evidence linking body weight and other markers of obesity to adverse health outcomes. *Diabetes Obes. Metab.* **27** (Suppl 2), 3–19. 10.1111/dom.16263 (2025).
9. Drucker, D. J. GLP-1 physiology informs the pharmacotherapy of obesity. *Mol. Metab.* **57**, 101351. 10.1016/j.molmet.2021.101351 (2022).
10. Jalleh, R. J. et al. Clinical Consequences of Delayed Gastric Emptying With GLP-1 Receptor Agonists and Tirzepatide. *J. Clin. Endocrinol. Metab.* **110**, 1–15. 10.1210/clinem/dgae719 (2024).
11. Wilding, J. P. H. et al. Once-Weekly Semaglutide in Adults with Overweight or Obesity. *N Engl. J. Med.* **384**, 989–1002. 10.1056/NEJMoa2032183 (2021).

12. Lincoff, A. M. et al. Semaglutide and Cardiovascular Outcomes in Obesity without Diabetes. *N Engl. J. Med.* **389**, 2221–2232. 10.1056/NEJMoa2307563 (2023).
13. Zhang, F. et al. Recombinant human GLP-1 beinaglutide regulates lipid metabolism of adipose tissues in diet-induced obese mice. *iScience* **24**, 103382. 10.1016/j.isci.2021.103382 (2021).
14. Basdas, R. et al. Semaglutide Modulates Proinflammatory Epicardial Adipogenesis With Paracrine Effects on hiPSC-Atrial Cardiomyocytes. *JACC Basic. Transl Sci.* **10**, 101277. 10.1016/j.jacbts.2025.03.009 (2025).
15. Kamrul-Hasan, A. B. M. et al. Effect of beinaglutide, a thrice-daily GLP-1 receptor agonist, on body weight and metabolic parameters: A systematic review and meta-analysis. *World J. Diabetes*. **16**, 103244. 10.4239/wjd.v16.i5.103244 (2025).
16. Soto-Catalán, M. et al. Semaglutide Improves Liver Steatosis and De Novo Lipogenesis Markers in Obese and Type-2-Diabetic Mice with Metabolic-Dysfunction-Associated Steatotic Liver Disease. *Int. J. Mol. Sci.* **25** 10.3390/ijms25052961 (2024).
17. Li, Q. & Spalding, K. L. The regulation of adipocyte growth in white adipose tissue. *Front. Cell. Dev. Biol.* **10**, 1003219. 10.3389/fcell.2022.1003219 (2022).
18. Cavaliere, G. et al. From Obesity-Induced Low-Grade Inflammation to Lipotoxicity and Mitochondrial Dysfunction: Altered Multi-Crosstalk between Adipose Tissue and Metabolically Active Organs. *Antioxid. (Basel)*. **12** 10.3390/antiox12061172 (2023).
19. Sun, K., Li, X. & Scherer, P. E. Extracellular Matrix (ECM) and Fibrosis in Adipose Tissue: Overview and Perspectives. *Compr. Physiol.* **13**, 4387–4407. 10.1002/cphy.c220020 (2023).
20. Kawai, T., Autieri, M. V. & Scalia, R. Adipose tissue inflammation and metabolic dysfunction in obesity. *Am. J. Physiol. Cell. Physiol.* **320**, C375–C391. 10.1152/ajpcell.00379.2020 (2021).
21. Crewe, C., An, Y. A. & Scherer, P. E. The ominous triad of adipose tissue dysfunction: inflammation, fibrosis, and impaired angiogenesis. *J. Clin. Invest.* **127**, 74–82. 10.1172/JCI88883 (2017).
22. Chakarov, S., Bleriot, C. & Ginhoux, F. Role of adipose tissue macrophages in obesity-related disorders. *J. Exp. Med.* **219** 10.1084/jem.20211948 (2022).
23. Shaikh, S. R., Beck, M. A., Alwarawrah, Y. & MacIver, N. J. Emerging mechanisms of obesity-associated immune dysfunction. *Nat. Rev. Endocrinol.* **20**, 136–148. 10.1038/s41574-023-00932-2 (2024).
24. Sun, K., Tordjman, J., Clement, K. & Scherer, P. E. Fibrosis and adipose tissue dysfunction. *Cell. Metab.* **18**, 470–477. 10.1016/j.cmet.2013.06.016 (2013).
25. Sasaki, N., Ueno, Y., Ozono, R., Nakano, Y. & Higashi, Y. Insulin resistance in adipose tissue and fatty liver, but not fat mass, are involved in worsening glycaemic status: The Hiroshima study on glucose metabolism and cardiovascular diseases. *Diabetes Obes. Metab.* **27**, 3025–3035. 10.1111/dom.16307 (2025).
26. Petersen, M. C. & Mittendorfer, B. Dysfunctional adipose tissue and skeletal muscle insulin resistance: Cause and effect or two sides of the same coin? *Obes. (Silver Spring)*. **31**, 1185–1187. 10.1002/oby.23750 (2023).

27. Kleiboeker, B. et al. Adipose tissue peroxisomal lipid synthesis orchestrates obesity and insulin resistance through LXR-dependent lipogenesis. *Mol. Metab.* **82**, 101913. 10.1016/j.molmet.2024.101913 (2024).
28. Auguet, T. et al. Downregulation of lipogenesis and fatty acid oxidation in the subcutaneous adipose tissue of morbidly obese women. *Obes. (Silver Spring)*. **22**, 2032–2038. 10.1002/oby.20809 (2014).
29. Martins, F. F. et al. Semaglutide (GLP-1 receptor agonist) stimulates browning on subcutaneous fat adipocytes and mitigates inflammation and endoplasmic reticulum stress in visceral fat adipocytes of obese mice. *Cell. Biochem. Funct.* **40**, 903–913. 10.1002/cbf.3751 (2022).
30. Jonker, J. W. et al. A PPARγ–FGF1 axis is required for adaptive adipose remodelling and metabolic homeostasis. *Nature* **485**, 391–394. 10.1038/nature10998 (2012).
31. Sancar, G. et al. FGF1 and insulin control lipolysis by convergent pathways. *Cell Metab* 34, 171–183 e176, (2022). 10.1016/j.cmet.2021.12.004
32. Saha, P. K. et al. The microRNA miR-30a blocks adipose tissue fibrosis accumulation in obesity. *J. Clin. Invest.* **135** 10.1172/JCI175566 (2025).
33. Chen, H. J. et al. Adipose extracellular matrix deposition is an indicator of obesity and metabolic disorders. *J. Nutr. Biochem.* **111**, 109159. 10.1016/j.jnutbio.2022.109159 (2023).
34. Dambrova, M. et al. Acylcarnitines: Nomenclature, Biomarkers, Therapeutic Potential, Drug Targets, and Clinical Trials. *Pharmacol. Rev.* **74**, 506–551. 10.1124/pharmrev.121.000408 (2022).
35. Hussein, N. A. et al. Liraglutide treatment and acylcarnitine profiles in Egyptian obese insulin-resistant females. *Eur. J. Pharmacol.* **891**, 173668. 10.1016/j.ejphar.2020.173668 (2021).
36. Zemski Berry, K. A. et al. Oxidised phosphatidylcholine induces sarcolemmal ceramide accumulation and insulin resistance in skeletal muscle. *Diabetologia* **67**, 2819–2832. 10.1007/s00125-024-06280-8 (2024).
37. Wang, G. et al. Enhancing de novo ceramide synthesis induced by bisphenol A exposure aggravates metabolic derangement during obesity. *Mol. Metab.* **73**, 101741. 10.1016/j.molmet.2023.101741 (2023).
38. Eichelmann, F. et al. Deep Lipidomics in Human Plasma: Cardiometabolic Disease Risk and Effect of Dietary Fat Modulation. *Circulation* **146**, 21–35. 10.1161/CIRCULATIONAHA.121.056805 (2022).
39. Tol, M. J. et al. Dietary control of peripheral adipose storage capacity through membrane lipid remodelling. *Nat. Metab.* **7**, 1424–1442. 10.1038/s42255-025-01320-y (2025).
40. Huang, K. P. et al. Sex differences in response to short-term high fat diet in mice. *Physiol. Behav.* **221**, 112894. 10.1016/j.physbeh.2020.112894 (2020).

Figures

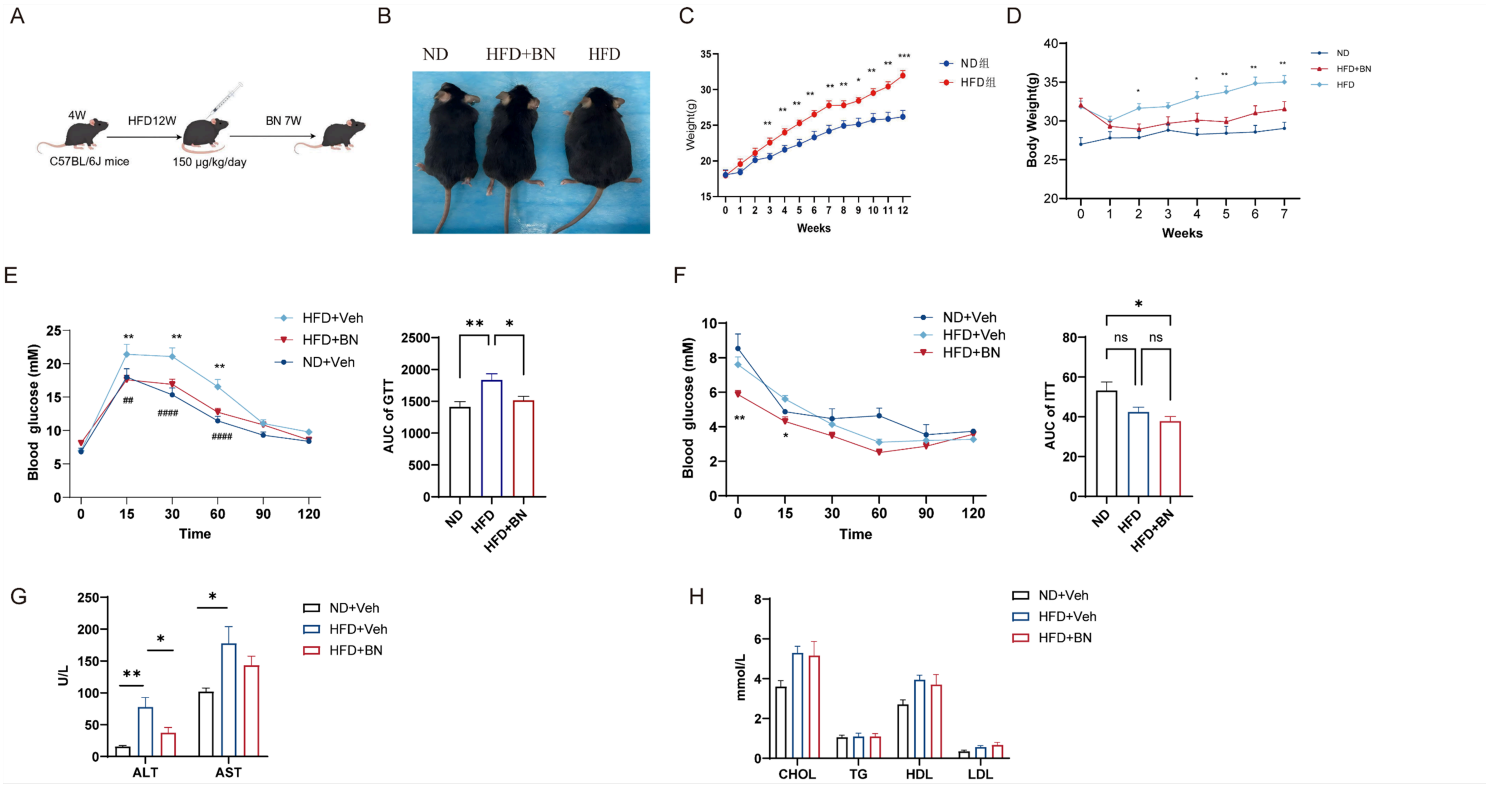


Figure 1

Beinaglutide partially alleviates HFD-induced obesity and metabolic dysfunction. **A** Schematic of the experimental design. C57BL/6J mice were fed a high-fat diet (HFD) for 12 weeks to establish diet-induced obesity, followed by beinaglutide (BN, 150 μg/kg/day) treatment for 7 weeks. **B** Representative gross appearance of mice from each group. **C** Body-weight changes during the 12-week HFD modelling period, n = 10. **D** Body-weight changes during the 7-week BN intervention period, n = 6. **E** Glucose tolerance test (GTT) curves and area under the curve (AUC) analysis, n = 6. **F** Insulin tolerance test (ITT) curves and AUC analysis, n = 6. **G** Serum alanine aminotransferase (ALT) and aspartate aminotransferase (AST) levels, n = 6. **H** Serum total cholesterol (CHOL), triglyceride (TG), high-density lipoprotein cholesterol (HDL), low-density lipoprotein cholesterol (LDL) levels, n = 6. Data are presented as mean ± SEM; Body weight changes (C, D) and GTT/ITT curves (E, F) were analyzed using two-way repeated-measures ANOVA. AUC values and serum biochemical parameters (G, H) were analyzed using one-way ANOVA followed by Tukey's multiple comparisons test. Statistical methods are described in Methods. *P < 0.05, **P < 0.01, ***P < 0.001; ns, not significant.

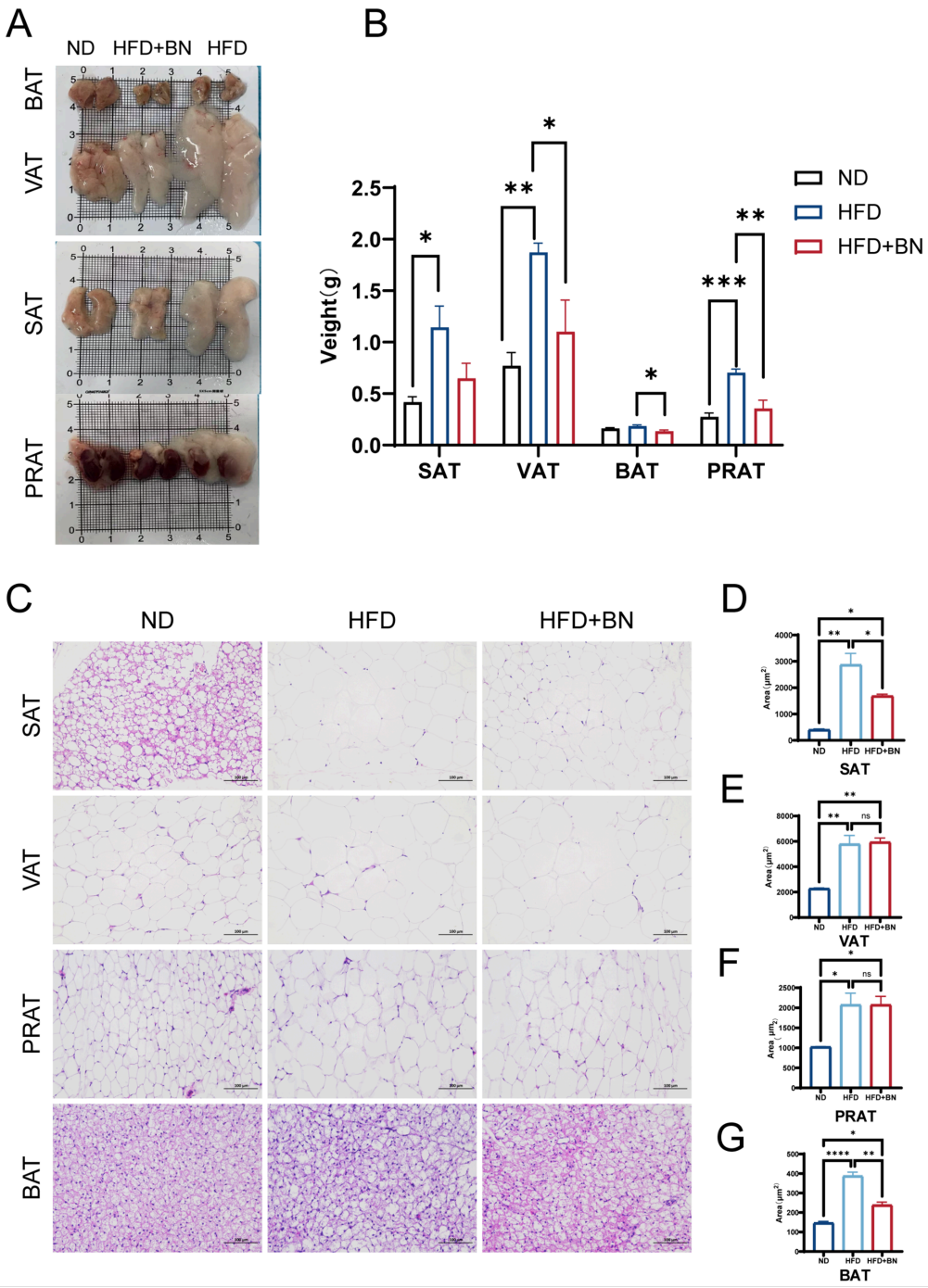


Figure 2

Beinaglutide improves HFD-induced morphological alterations in adipose tissues.

A、**B** Representative gross morphology and tissue weights of SAT, VAT, PRAT and BAT from mice in the ND, HFD and HFD+BN groups.**C** Representative H&E-stained images of SAT, VAT, PRAT and BAT. Scale bar, 100 μm.**(D–G)**Quantification of mean adipocyte area in SAT, VAT, PRAT and BAT.All data are

presented as mean ± SEM. n = 6 mice per group. Statistical analysis was performed using one-way ANOVA, followed by Tukey's multiple comparisons test where appropriate. *P < 0.05, **P < 0.01, ***P < 0.001 and ****P < 0.0001

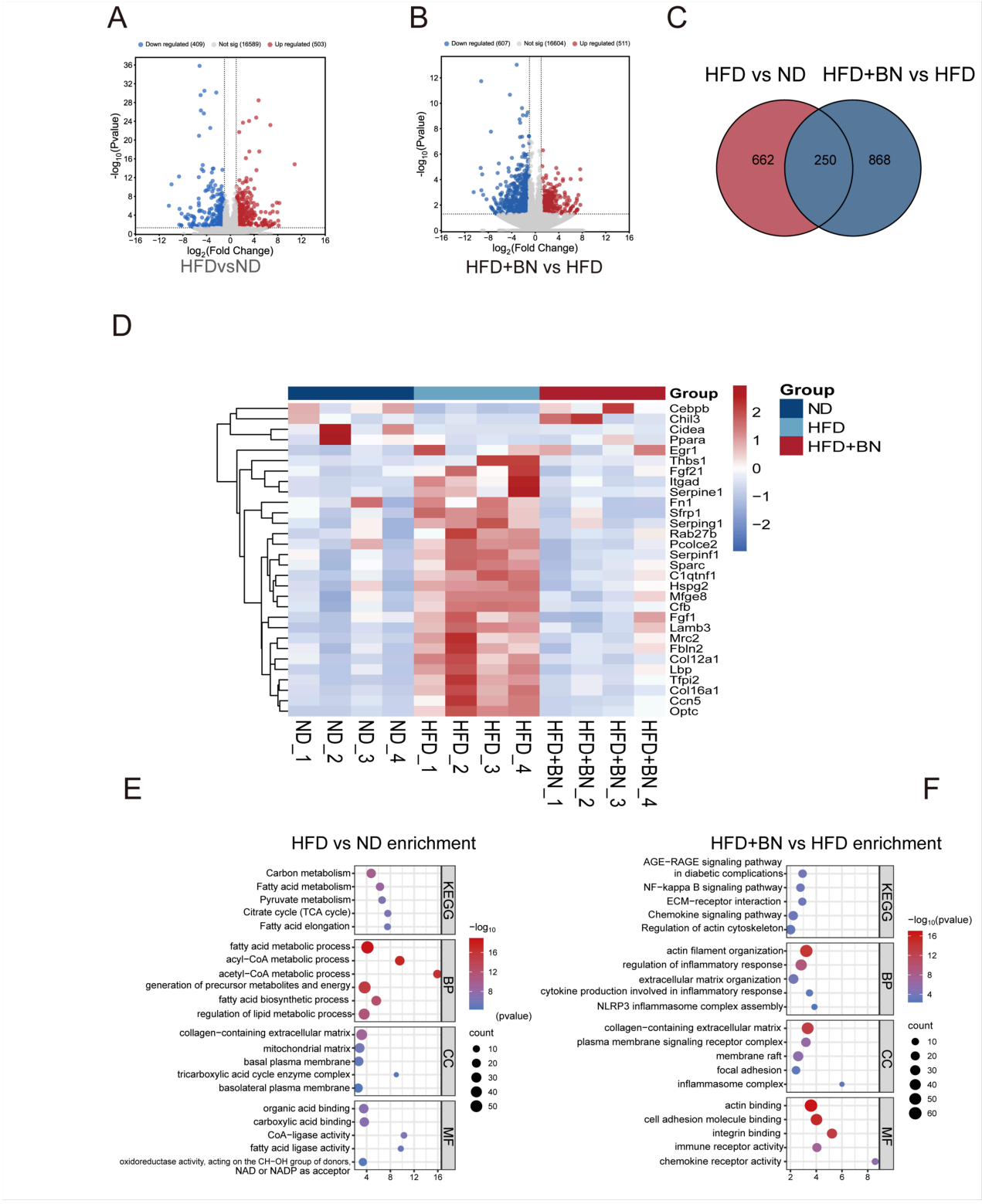


Figure 3

BN-associated transcriptional responses in abdominal subcutaneous adipose tissue are enriched for inflammatory and ECM-remodelling programs. **A** Volcano plot showing differentially expressed genes in HFD vs ND. Red denotes up regulated genes, blue denotes down regulated genes and grey denotes non-significant genes. **B** Volcano plot showing differentially expressed genes in HFD+BN vs HFD. Red denotes up regulated genes, blue denotes down regulated genes and grey denotes non-significant genes. **C** Venn diagram showing the overlap of differentially expressed genes between HFD vs ND and HFD+BN vs HFD comparisons. **D** Heatmap of representative genes altered by HFD and showing a reversal trend after BN treatment. Colours indicate gene-wise standardized relative expression levels. **E** KEGG and GO enrichment analysis of differentially expressed genes in HFD vs ND. **F** KEGG and GO enrichment analysis of differentially expressed genes in HFD+BN vs HFD.n = 4 mice per group. Criteria for differential expression and enrichment analysis are described in Methods. Dot size indicates the number of enriched genes, and colour indicates -log10(P value).

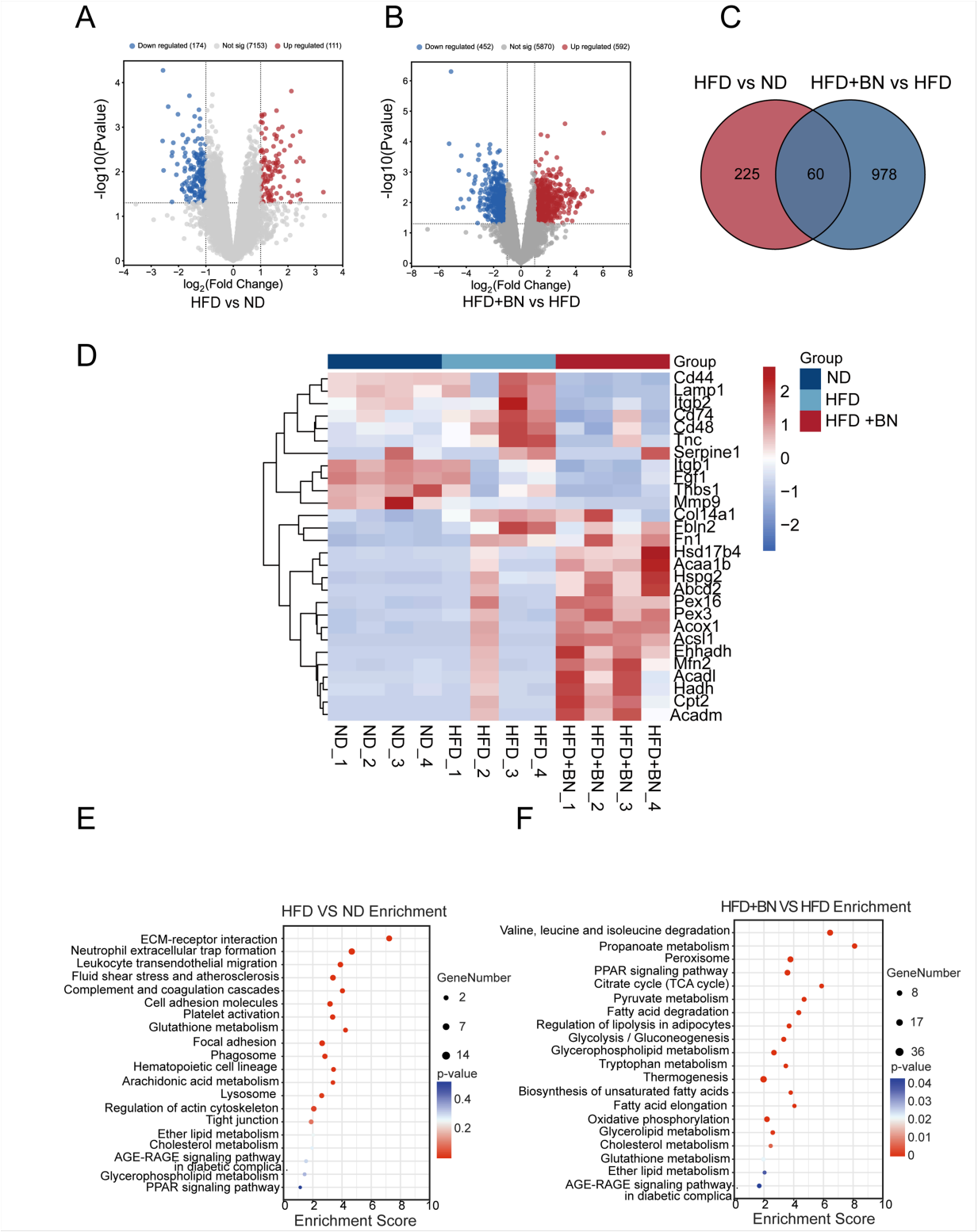


Figure 4

BN-associated proteomic changes in abdominal subcutaneous adipose tissue point to PPAR/peroxisome and fatty acid oxidation pathways. **A** Volcano plot of differentially expressed proteins in HFD vs ND, n = 4. **B** Volcano plot of differentially expressed proteins in HFD+BN vs HFD, n = 4. **C** Venn analysis of differentially expressed proteins between the two comparisons, n = 4. **D** Heatmap of representative proteins related to adipose-tissue microenvironment remodelling, fatty acid oxidation

and peroxisomal function, n = 4. Colours indicate protein-wise standardized relative abundance.**E**KEGG enrichment analysis of differentially expressed proteins in HFD vs ND, n = 4.**F**KEGG enrichment analysis of differentially expressed proteins in HFD+BN vs HFD, n = 4.Dot size indicates the number of enriched proteins, and colour indicates P value. Differential expression and enrichment analyses are described in Methods.

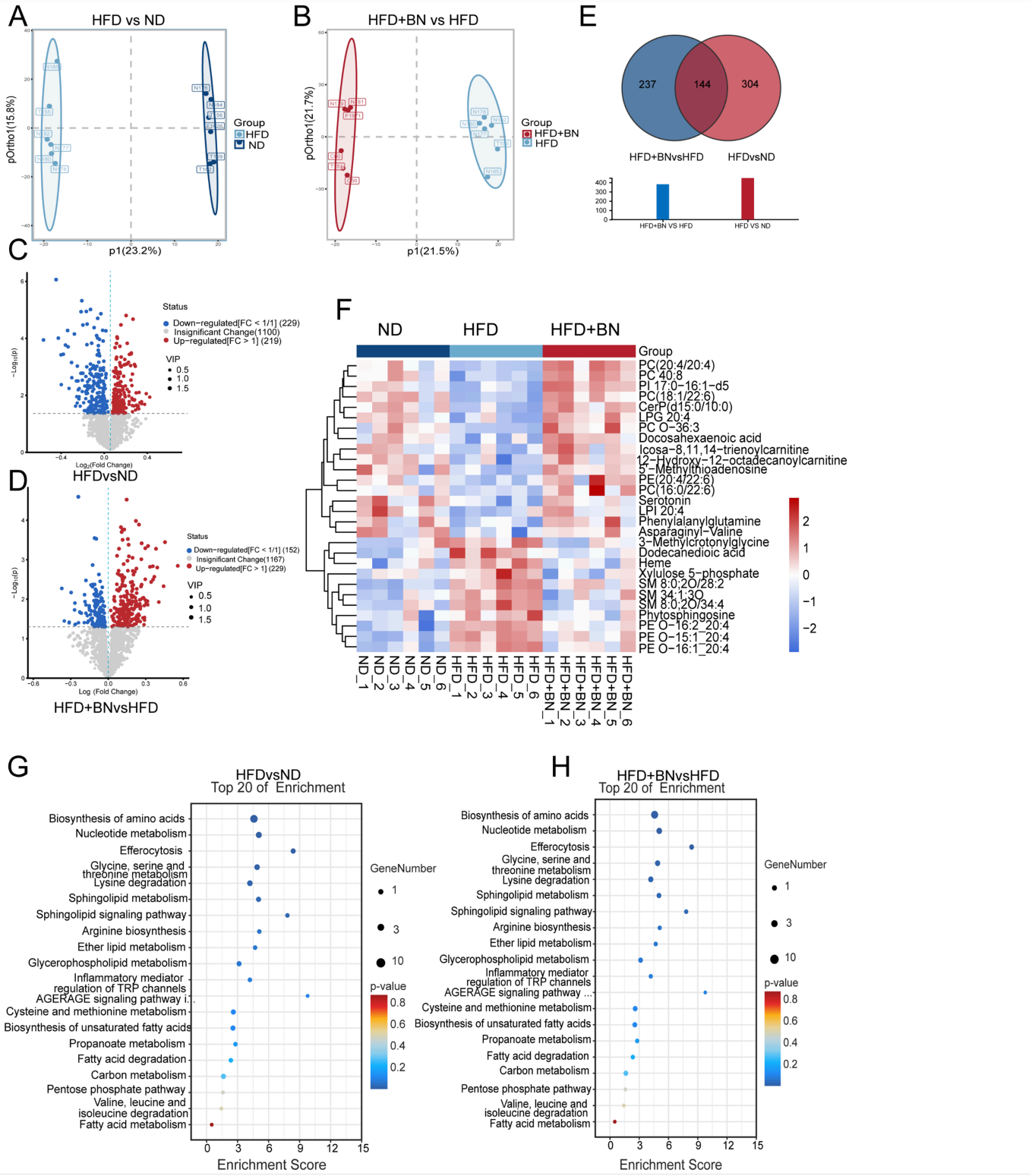


Figure 5

BN-associated metabolic alterations in abdominal subcutaneous adipose tissue point to membrane lipid, sphingolipid and fatty acid oxidation-related remodelling. **A** OPLS-DA score plot for HFD vs ND. **B** OPLS-DA score plot for HFD+BN vs HFD. **C** Volcano plot of differential metabolites in HFD vs ND. **D** Volcano plot of differential metabolites in HFD+BN vs HFD. **E** Venn analysis of differential metabolites between the two comparisons. **F** Heatmap of representative differential metabolites. Colours indicate metabolite-wise standardized relative abundance. **G** KEGG pathway analysis of differential metabolites in HFD vs ND. **H** KEGG pathway analysis of differential metabolites in HFD+BN vs HFD.n = 6 mice per group. Dot size indicates the number of enriched metabolites, and colour indicates P value. Differential metabolite screening and enrichment analyses are described in Methods.

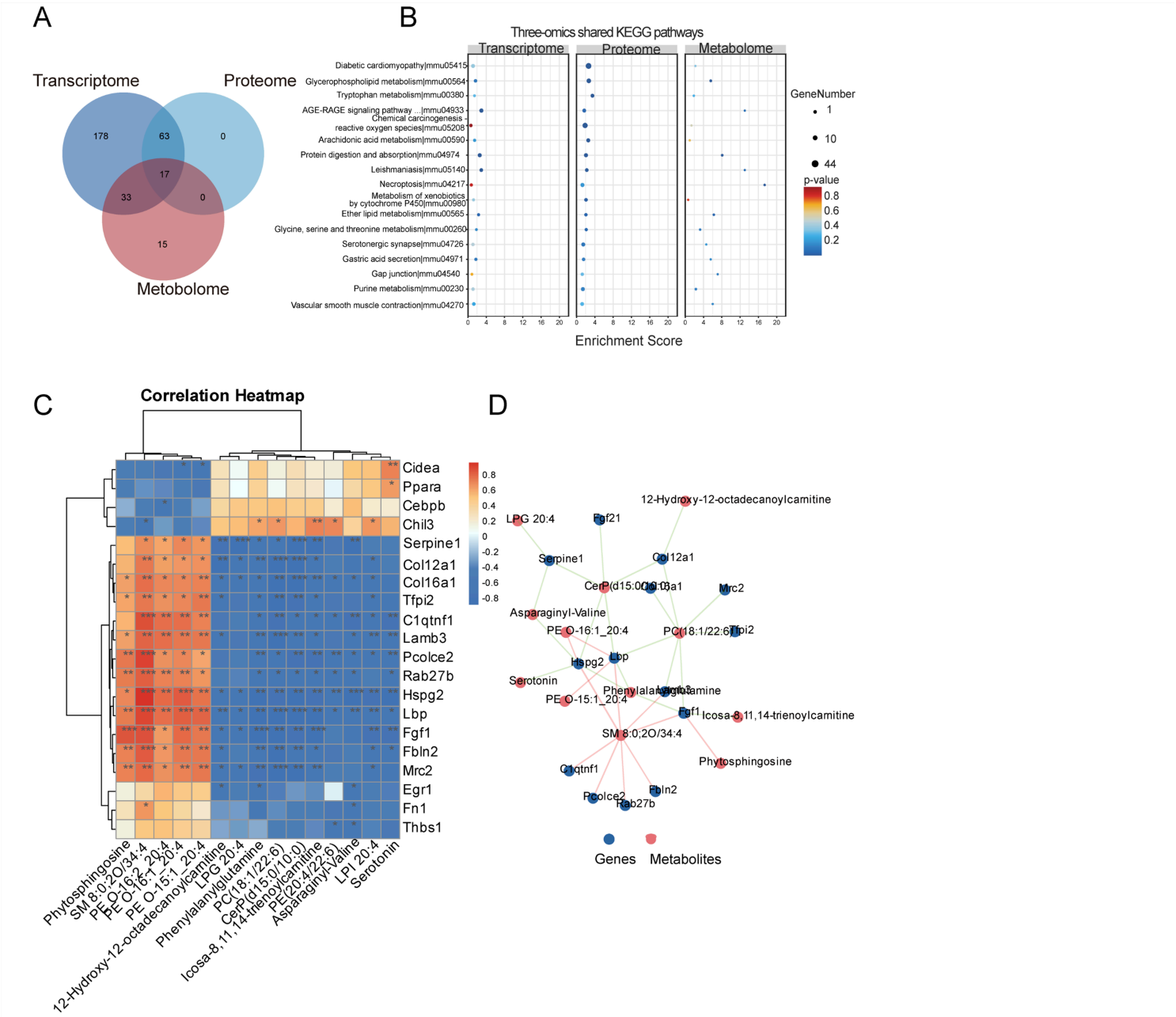


Figure 6

Multi-omics integration links BN-associated molecular responses to lipid metabolism, metabolic stress and inflammatory processes. **A** Venn diagram showing the overlap of KEGG pathways among transcriptomic, proteomic and metabolomic analyses. **B** Grouped bubble plot of KEGG pathways shared across the three omics layers. Dot size indicates the number of enriched genes, proteins or metabolites, and dot colour indicates the enrichment P value derived from the HFD+BN vs HFD comparison. **C** Correlation heatmap between key genes and differential metabolites. Colours indicate correlation coefficients; *p < 0.05, **p < 0.01. **D** Candidate gene-metabolite correlation network. Blue nodes represent genes and red nodes represent metabolites. Red edges indicate positive correlations, whereas green edges indicate negative correlations. Edge thickness represents the magnitude of the correlation coefficient, with thicker edges indicating stronger correlations. Correlation analyses were performed across all samples. Statistical methods are described in the Methods.All omics measurements were obtained from biologically independent animals, with n = 4 per group.

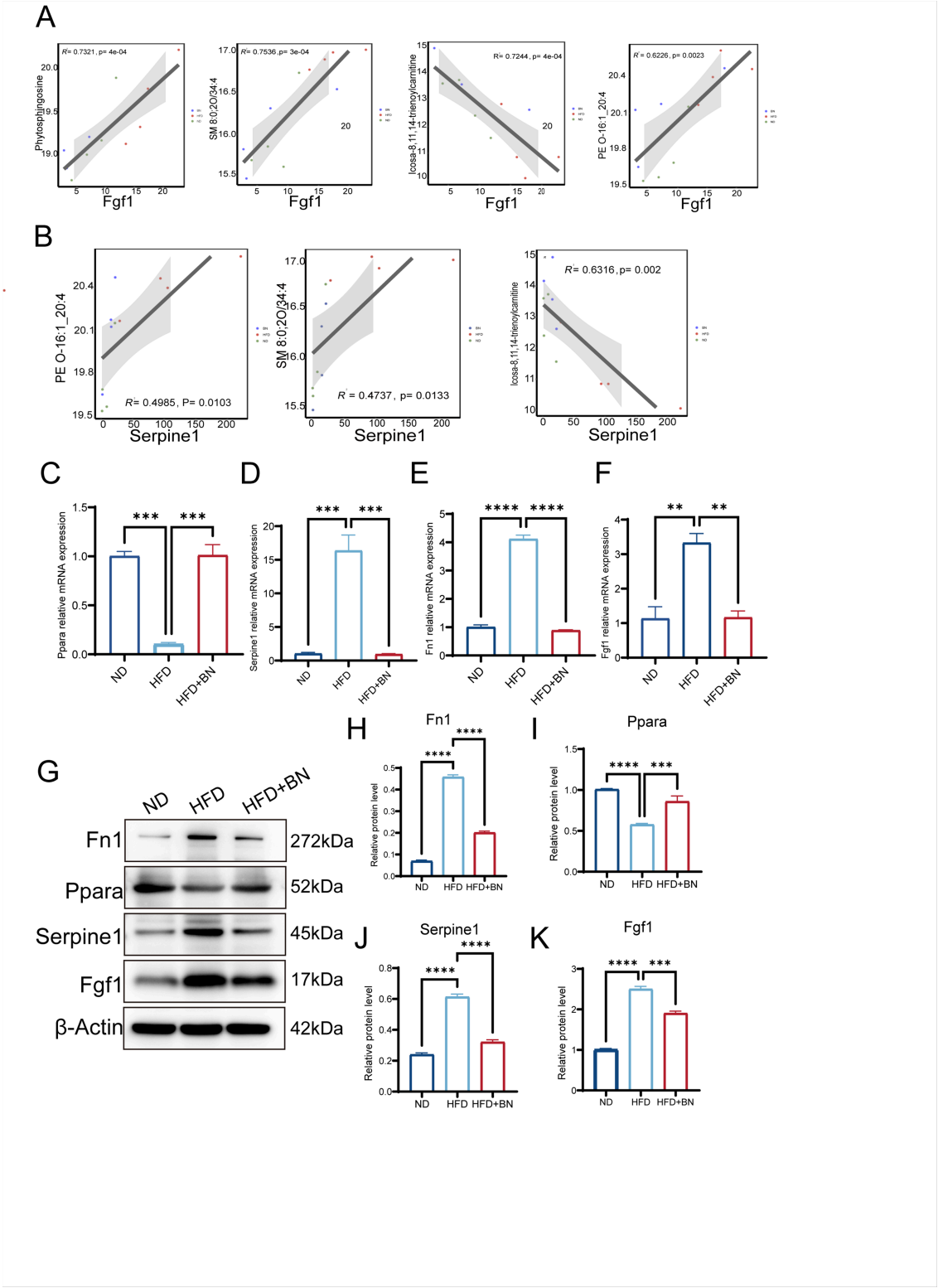


Figure 7

Validation of candidate gene expression and metabolic associations.

A,B Representative scatter plots selected from the gene-metabolite correlation network in Figure 6. A shows the correlations of Fgf1 with Icosa-8,11,14-trienoylcarnitine, PE O-16:1/20:4, Phytosphingosine and SM 8:0;2O/34:4. B shows the correlations of Serpine1 with Icosa-8,11,14-trienoylcarnitine, PE O-

16:1/20:4 and SM 8:0;2O/34:4. **C-F**RT-qPCR analysis of the relative expression levels of Ppara, Serpine1, Fn1 and Fgf1 in abdominal subcutaneous adipose tissue. **G**Representative Western blot bands for PPARα, FN1, SERPINE1 and FGF1 protein expression. **H-K**Quantification of PPARα, FN1, SERPINE1 and FGF1 protein levels. The western blot images are cropped for presentation; the corresponding full-length, uncropped blots are provided in Supplementary Figs. A5 and A6.Data are presented as mean ± SEM, n = 3 per group. *P < 0.05, **P < 0.01, ***P < 0.001; ns, not significant.

Supplementary Files

This is a list of supplementary files associated with this preprint. Click to download.

- Supplementarydocuments.zip
- Supplementary.docx